

Teraflop per second gravitational lensing ray-shooting using graphics processing units¹

Alexander C. Thompson, Christopher J. Fluke*,
David G. Barnes and Benjamin R. Barsdell

*Centre for Astrophysics and Supercomputing, Swinburne University of Technology,
P.O. Box 218, Hawthorn, Victoria 3122, Australia*

Abstract

Gravitational lensing calculation using a direct inverse ray-shooting approach is a computationally expensive way to determine magnification maps, caustic patterns, and light-curves (e.g. as a function of source profile and size). However, as an easily parallelisable calculation, gravitational ray-shooting can be accelerated using programmable graphics processing units (GPUs). We present our implementation of inverse ray-shooting for the NVIDIA G80 generation of graphics processors using the NVIDIA Compute Unified Device Architecture (CUDA) software development kit. We also extend our code to multiple-GPU systems, including a 4-GPU NVIDIA S1070 Tesla unit. We achieve sustained processing performance of 182 Gflop/s on a single GPU, and 1.28 Tflop/s using the Tesla unit. We demonstrate that billion-lens microlensing simulations can be run on a single computer with a Tesla unit in timescales of order a day without the use of a hierarchical tree code.

Key words: Gravitational Lensing, Methods: Numerical
PACS: 95.75.Pq, 98.62.Sb, 98.62.-g

1 Introduction

Gravitational microlensing is the study of the deflection of light by matter in a regime where high magnification and multiple-imaging occurs, but the individual micro-images are not resolvable. This includes high magnification events

¹ Research undertaken as part of the Commonwealth Cosmology Initiative (CCI: www.thecci.org), an international collaboration supported by the Australian Research Council

* Corresponding author. Tel.: +61 (0)3 9214 5828; fax: +61 (0)3 9214 8797.
Email address: cfluke@swin.edu.au (Christopher J. Fluke).

due to lenses in the Galactic bulge and halo (Alcock et al. 1993; Aubourg et al. 1993; Udalski et al. 1993), and microlensing by compact objects within macro-lenses at cosmological distances (Vanderriest et al. 1989; Irwin et al. 1989). While Galactic microlensing projects have focused on searches for dark matter and the detection of planets, cosmological microlensing has led to advances in the understanding of stellar mass functions, mean stellar masses, and the structure of quasars, including constraints on the physical size of the emission regions at different wavelengths. See Wambsganss (2006), Kochanek et al. (2007), Gould (2008), and Mao (2008) for recent reviews.

The standard signature of cosmological microlensing, especially when applied to observations of active galactic nuclei, is an uncorrelated change in brightness of a single macro-image within a multiply-imaged system (Schneider & Weiss 1987). Intrinsic variation in source flux is seen as a correlated change in the brightness of all the images, separated by the (macro)lensing time-delay. Such observations require accurate light curves to be obtained over long time periods, in many cases decades, as there is a wide variation in the time delay: 2 – 30 hours for the quadruple-lensed Q2237+0305 (Vakulik et al. 2006) and 423 days for Q0957+561 (Hjorth et al. 2002) – see Saha et al. (2006) and Oguri (2007) for further examples.

Determination of the source size, source intensity profile, and physical properties of the microlenses (mass function, mean mass), requires a statistical comparison between observed light curves and microlensing models. This is achieved through the use of the gravitational lens equation:

$$\mathbf{y} = \mathbf{x} - \boldsymbol{\alpha}(\mathbf{x}), \quad (1)$$

which relates the two-dimensional locations of a source, \mathbf{y} , and an image, \mathbf{x} , with the deflection angle term, $\boldsymbol{\alpha}(\mathbf{x})$, dependent on the arrangement of lenses. A common choice for microlensing is the many-Schwarzschild lens model:

$$\boldsymbol{\alpha}(\mathbf{x}) = \sum_{i=1}^{N_*} m_i \frac{(\mathbf{x} - \mathbf{x}_i)}{|\mathbf{x} - \mathbf{x}_i|^2} \quad (2)$$

for N_* lenses with masses, m_i , at positions \mathbf{x}_i . The magnification, μ , due to a gravitational lens system is

$$\mu = 1 / \det \mathbf{A} \quad (3)$$

where $\mathbf{A} = \partial \mathbf{y} / \partial \mathbf{x}$ is the Jacobian matrix of equation (1), which measures the areal distortion between the image and source planes.

While an image position maps uniquely to a source location ($\mathbf{x} \rightarrow \mathbf{y}$ is a one-to-one mapping), the converse is not true ($\mathbf{y} \rightarrow \mathbf{x}$ is a one-to-many mapping). Except for a limited number of special cases [see Schneider et al. (1992) for examples], the lens equation is not invertible. In the cosmological microlensing case, where many millions of individual stars may contribute to the observed

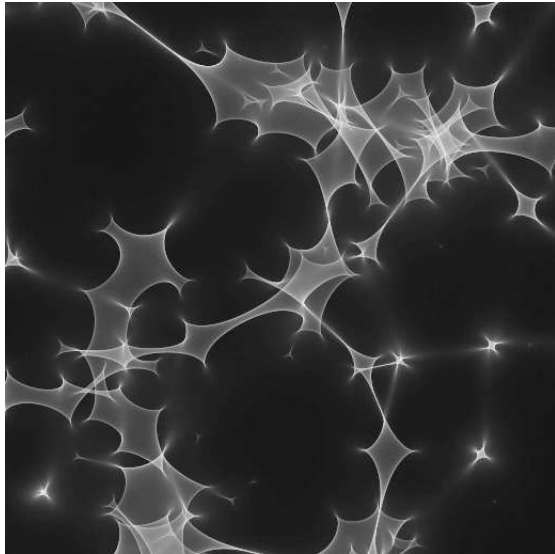


Fig. 1. A sample microlensing magnification map generated with a pair of NVIDIA GeForce 8800GT graphics cards. For model parameters: $N_* = 100$ lenses, $N_{\text{pix}} = 1024^2$ pixels in the source plane, and $N_{\text{av}} = 1000$ light rays per source pixel (on average), the processing time was 135 s. See section 2 for details.

magnification of a macro-image, it is more common to use a numerical technique to solve for μ over a finite region of the source plane – a magnification map – rather than attempting to find all image locations from equation (1) for a given source position (e.g. Paczyński 1986).

Inverse ray-shooting provides the most straightforward means to obtain magnification maps for an arbitrary lens distribution [see Kayser et al. (1986) and Schneider & Weiss (1986; 1987) for early versions of this technique]. Inverse ray-shooting follows a large number (typically millions) of light rays backwards from the observer, through the lens plane to the source plane, which is represented as a pixellated grid. The number of light rays falling in each pixel, N_{ij} , compared to the (average) number if there was no lensing, N_{av} , gives an estimate of the per-pixel magnification:

$$\mu_{ij} = N_{ij}/N_{\text{av}}. \quad (4)$$

A typical magnification map is shown in Figure 1, with the characteristic pattern of caustics clearly visible. Caustics are regions of high magnification – formally those points where $\det \mathbf{A} = 0$. The relative motion of the observer, lens plane and source imparts an effective transverse velocity to the source, causing it to move across the caustic network, and resulting in a time-varying change in source brightness. Accordingly, a sample light curve is generated by moving a source profile across a simulated caustic network, and converting the magnification at each point to a magnitude change.

Statistical investigations of cosmological microlensing require the generation

of many sample light curves, however, the creation of magnification maps poses a significant computational challenge. The time to calculate a magnification map is directly proportional to the number of pixels in the source plane (N_{pix}), the number of microlenses (N_*), and the number of floating point operations¹ (N_{flop}) per deflection calculation. As a Monte Carlo technique, the computation time is extended in direct proportion to N_{av} , which sets the accuracy of calculated magnifications, and the number of repeat (n) map generations. Long compute times — $O(\text{days–months})$ — limit the scope to vary the input parameters, such as the initial stellar mass function, mean stellar mass, and source grid resolution. To keep computation times feasible for a direct implementation of the inverse ray-shooting method, the product $\Phi = n \times N_{\text{flop}} \times N_{\text{pix}} \times N_* \times N_{\text{av}}$ historically has been constrained to $\lesssim O(10^{16})$.

A number of approaches have been developed to overcome the processing time problem. Wambsganss (1990; 1999) used a hierarchical tree code (Barnes & Hut 1986), where lenses are treated differently depending on their distances from the light ray: lenses at a similar distance from a ray are grouped together and replaced with a single pseudo-lens of higher mass, effectively reducing the N_* factor. This introduces a slight error in the magnification map, which can be reduced by including higher order moments of the mass distribution. A parallel version of the tree code, suitable for running billion-lens calculations on a parallel computing cluster – a region of parameter size previously unavailable to microlensing codes – has been implemented by Garsden & Lewis (2009).

Mediavilla et al. (2006) used a lattice of polygonal cells to map areas of the image plane to source plane pixels, rather than using a regular grid in the source plane. This greatly reduces N_{av} , resulting in a $\sim 100\times$ speed-up to reach a given accuracy compared to standard inverse ray-shooting, however, preparing an appropriate polygonal lattice introduces a significant computation overhead.

A limitation of Monte Carlo-style methods is that many more magnification values, N_{pix} , are constructed than may actually be required (e.g. to form a single light curve). A slightly larger (angular) size must be used for the image plane than for the source plane, as light rays at large impact parameters can be deflected into the source plane, contributing flux that would otherwise be lost. Consequently, more light rays must be generated than will actually fall within the source grid. Additionally, the finite source grid resolution means that true point source magnifications cannot be accurately calculated. To avoid these issues, Lewis et al. (1993) and Witt (1993) independently developed approaches based on imaging an infinite line in the source plane, which maps to a continuous, infinite line in the image plane, plus a number of closed loops

¹ We use the notation: flop = floating point operation; 1 Gflop/s = 1 Gigaflop per second; and 1 Tflop/s = 1 Teraflop per second.

- one for each microlens. Wyithe & Webster (1999) developed this technique further for extended sources.

In this work, we demonstrate that the redeployment of the direct inverse ray-shooting algorithm on modern, programmable graphics processing units (GPUs) can dramatically speed-up the calculation of microlensing magnification maps, without the programming overheads of implementing a more complex code. GPUs are macroscopic semiconductor arrays designed to accelerate the rendering of three-dimensional geometry for display on two-dimensional computer screens. Most modern computers contain a GPU, either on the system board or on a peripheral graphics card, which now regularly provide at least an order of magnitude greater raw computational power than the central processing unit (CPU). Rendering on-screen pixels is a highly parallel task, and this is reflected in the GPU architecture. Modern GPUs are primarily composed of stream processors, which are individual arithmetic logic units (ALUs) grouped in sets and controlled by an instruction scheduler with associated shared memory. Consequently, algorithms that lend themselves to the “stream processing” paradigm, where many individual data-streams all undergo identical operations, can be moved to the GPU, resulting in significantly shorter computation times.

On-going improvements in the performance of programmable graphics hardware, combined with the notion of general purpose computation on GPUs (GPGPU), is heralding a revolution in scientific computing (Fournier & Fussell 1988; Tomov et al. 2003; Venkatasubramanian 2003; Owens et al. 2005). The two major graphics processor manufacturers, NVIDIA and AMD, support GPGPU by providing software development kits for stream computing. NVIDIA introduced its Compute Unified Device Architecture² (CUDA) in 2006. CUDA is an extension (via compiler directives) of the standard C programming language, designed to simplify the process of GPGPU programming by abstracting the process of writing GPU code. AMD’s “ATI Stream” technology is based on an evolved form of Brook.³ Brook was one of the first GPU languages that went beyond the standard shader languages (particularly Cg⁴ and GLSL⁵) to provide general purpose computing capabilities. Both CUDA and ATI Stream allow the programmer to define functions that are executed in parallel on one or more GPUs attached to a system.

Astronomers are just beginning to consider the advantages that GPUs can offer for computation. Early work has focused on a few well-known algorithms, with gravitational N-body simulations receiving particular attention. Nyland et al. (2004) were the first to attempt to move the expensive $O(N^2)$ inter-

² <http://www.nvidia.com/cuda>

³ <http://www-graphics.stanford.edu/projects/brookgpu/>

⁴ <http://www.nvidia.com>

⁵ <http://opengl.org>

body force calculations performed during an N-body simulation from the CPU to the GPU, work that was later followed by Portegies Zwart et al. (2007). Both groups found performance increases of $O(10)$ times, demonstrating the significant potential of GPUs, but their efforts were inhibited by the use of inflexible shader languages. The arrival of GPGPU languages improved the situation greatly, and measured performances of $O(100)$ times over CPU implementations led to a flurry of work in the area using BrookGPU (Elsen et al. 2007) and CUDA (Hamada & Iitaka 2007; Belleman et al. 2007; Schive et al. 2007; Nyland et al. 2008; Moore et al. 2008). Other astronomy algorithms implemented on the GPU include radio-telescope signal correlation (Schaaf & Overeem 2004; Wayth et al. 2007; Harris et al. 2008; Ord et al. 2009) and the solution of Kepler’s equations (Ford 2008). GPUs have also been used for real-time visualisation of large datasets (Szalay et al. 2008).

We now describe the implementation of GPU-based, direct inverse ray-shooting code for microlensing experiments. We demonstrate the substantial performance gains in executing our implementation on a system containing one or two NVIDIA GeForce 8800 GT graphics cards, and on a system with an attached (external) NVIDIA S1070 Tesla unit. The remainder of this paper is organised as follows. In section 2 we describe both OpenMP (for multiple-core CPU systems) and our CUDA-based approach for single and multi-GPU systems. We compare processing performance via timing tests in section 3. In section 4, we consider advantages and limitations of GPGPU computing relevant to the ray-shooting case, and discuss applications of our approach, including computational steering.

2 Stream-processed ray-shooting

The inverse ray-shooting algorithm is an ideal candidate for moving to a GPU as it is “trivially parallelisable”: the deflection of a single light ray is independent of the deflection of all other light rays, and the deflection of a light ray due to one lens is independent of the deflection due to all other lenses. The former case can be treated by splitting up the total number of light rays, N_{ray} , into N_{batch} batches that are deflected in parallel. The latter case can be treated by recasting the lens equation as:

$$\mathbf{x} - \mathbf{y} = \sum_{t=1}^T \sum_{i=1}^{N_t} m_i \frac{(\mathbf{x} - \mathbf{x}_i)}{|\mathbf{x} - \mathbf{x}_i|^2} \quad (5)$$

where $\sum_{t=1}^T N_t = N_*$ for T parallel threads, and each processing step considers only a single light ray. Our final solution uses a combination of both parallel options.

The choice of parallel scheme necessitates a trade-off between memory usage and processing speed. Aggregate GPU speed depends on the following characteristics of the architecture: the number of stream processors, which determines how many independent parallel tasks can be performed (per GPU stream clock cycle); stream processor clock speed, which controls how many instructions can be operated on in a given time period; memory bandwidth, which specifies how quickly memory can be accessed, and is typically faster on the GPU than the CPU;⁶ and GPU memory (classified as either device, shared or register memory), which limits the amount of data that can be used for parallel processing.

2.1 An OpenMP solution

As a step towards the GPU implementation, we consider OpenMP.⁷ Processing threads are distributed amongst multiple CPUs on a single machine, with the run-time environment controlling thread allocation. Compiler directives indicate code blocks to be processed in parallel, requiring minimal changes to the overall program structure. In astronomy, OpenMP has been primarily used for gravitational and hydrodynamical simulations (e.g. Thacker 1999; Semelin & Combes 2005; Merz, Pen & Trac 2005; Thacker & Couchman 2006; and Mudryk & Murray 2009).

The OpenMP direct ray-shooting algorithm works as follows:

- (1) N_* lenses are generated on the CPU and stored in system memory.
- (2) N_{ray} light ray positions (\mathbf{x}) are randomly generated in serial on the CPU and stored in system memory;
- (3) Source coordinates are calculated in parallel, with light rays divided evenly between threads by OpenMP;
- (4) Once complete, a single thread maps the ray locations onto the source pixel grid in order to obtain the magnification map.

This approach avoided potential problems such as multiple threads attempting to write to the same memory location when updating deflection angles, inaccurate or slow random number generation (the standard `libc` random number generator `rand()` is not thread safe), and enables a simpler extension to GPU programming with CUDA. We note that this algorithm assumes that all lens positions can be stored in CPU memory at one time, which limits the range of N_* that we can use for timing tests in section 3.1.

⁶ e.g. the NVIDIA GeForce 8800 GT streams 57.6 GB/s, c.f. a typical high-end CPU with dual-channel DDR2-800 with 12.8 GB/s of memory bandwidth

⁷ <http://openmp.org>

2.2 GPU ray-shooting with CUDA

Our GPU ray-shooting algorithm operates in a similar manner to the OpenMP code, except that lens and light ray positions generated by the CPU and stored in the computer memory must be copied to and from the GPU's memory as part of each processing cycle. For our specific implementation, we chose CUDA over ATI Stream technology for two main reasons: (i) it is available on more architectures (i.e. Windows, Linux and Mac OS/X, compared to ATI Stream, which only supports Windows and Linux) and (ii) NVIDIA has been the first-to-market with desktop, GPGPU-specific, multi-Tflop/s products like the Tesla. The C function calls of the OpenMP code are replaced with calls to the CUDA library.

The GPU ray-shooting algorithm works as follows:

- (1) N_* lenses are generated on the CPU and loaded into GPU device memory;
- (2) N_{batch} light ray coordinates are randomly generated on the CPU and loaded into GPU device memory;
- (3) GPU computation is initialised; computation is split into groups of 128 threads (see below);
- (4) Each thread group loads 128 lenses and calculates deflection on 128 rays, this is repeated until all lenses and rays are exhausted;
- (5) Once computation on the GPU is complete, results are copied back from the GPU device memory to system memory;
- (6) CPU maps the ray locations onto the source pixel grid in order to obtain the magnification map;
- (7) Steps 2-6 repeated until N_{av} rays per source pixel is reached.

Ray coordinates are generated and processed in batches, as this minimises memory usage on the GPU while not reducing performance with a significantly large number of rays. For this work, N_{batch} was set to 2^{17} , as larger sizes did not increase performance. To maximise efficient use of the GPU device memory, source ray coordinates can overwrite the image ray coordinates, as they are still stored on the CPU memory. 128 threads are run per group, which improves throughput, while not exhausting the supply of registers and shared memory. The GPUs on the Tesla unit have more registers, allowing 256 threads per group. This number of 128 or 256 threads was chosen using the NVIDIA CUDA occupancy calculator⁸ to determine best utilisation of the GPU, and this number was confirmed with testing.

⁸ http://developer.download.nvidia.com/compute/cuda/CUDA_occupancy_calculator.xls

2.3 Multiple GPUs and the Tesla unit

To make use of multiple GPUs or a Tesla device, multiple CPU threads are used. One CPU thread is associated with each GPU, handling memory transfer to and from the device, and calls to device functions to perform computation. For our implementation, CPU thread management was performed by OpenMP, as it takes care of thread initialisation, destruction and synchronisation. The multiple GPU algorithm works as follows:

- (1) N_* lenses are generated on the CPU and loaded into all GPUs device memory;
- (2) $N_{\text{GPU}} \times N_{\text{batch}}$ light ray coordinates are randomly generated in serial on the CPU by the master thread and stored in N_{GPU} arrays;
- (3) N_{GPU} threads copy ray coordinates to the GPUs and GPU computation is initialised;
- (4) Computation is split into groups of 128 threads – computation on each GPU is independent of the others;
- (5) Each thread group loads 128 lenses and calculates deflection on 128 rays, this is repeated until all lenses and rays are exhausted;
- (6) Once computation on all GPUs is complete, results are copied back from the GPU device memory to system memory;
- (7) The master CPU thread maps the ray locations onto the source pixel grid in order to obtain the magnification map;
- (8) Steps 2-6 repeated until N_{av} rays per source pixel is reached.

While the best performance for our GPU algorithm was achieved when accessing only registers and shared memory, it is not possible to avoid either the transfer from CPU memory to GPU device memory, or from device to shared or register memory. While this may seem like a processing bottleneck, the high latency of a single access of device memory is offset by the significant gain due to multiple streams being able to access device memory in parallel.

3 Comparing the approaches

3.1 Timing Tests

To evaluate the relative performance of OpenMP and CUDA inverse ray-shooting codes, a number of timing tests were performed. We also implemented a single-CPU code: although the parameter space where this can be run is limited, it does provide a check on the accuracy of the parallel codes. The same base hardware was used throughout, comprising an Intel Q6600 Quad Core

Table 1

Hardware configurations used in the comparison of inverse ray-shooting codes. The memory column lists the total memory available for each processing option, which sets the problem size (N_* and N_{batch} light rays) that can be processed instantaneously.

Name	Description	Type	Memory
1CPU	Single thread on Intel Q6600	CPU	4 GB
4CPU	OpenMP with four threads on Intel Q6600 CPU	CPU	4 GB
1GPU	Single NVIDIA GeForce 8800 GT	GPU	512 MB
2GPU	Two NVIDIA GeForce 8800 GTs	GPU	2×512 MB
1TES	NVIDIA S1070 Tesla with 4 GPU cores	GPU	4×4 GB

CPU (2.4 GHz), with 4 GB of RAM and either two NVIDIA GeForce 8800 GTs or an NVIDIA S1070 Tesla unit connected via dual PCIe x8, or higher, buses. In Table 1, we provide a summary of the hardware configurations.

The 8800 GT comprises 112 stream processors, each running at 1.5 GHz, with a peak performance of 336 Gflop/s.⁹ This is much higher than a typical high-end CPU, such as the Intel Core 2 Quad Q6600, which is capable of 76.8 Gflop/s. The 8800 GT has 512 MB of memory, which can store up to 6.7×10^7 two-dimensional lens positions as 32-bit (i.e. single precision) floating point numbers. The Tesla S1070¹⁰ comprises four GPUs, each with 240 stream processors, running at at 1.296 GHz. The Tesla’s processing peak is 2.488 Tflop/s, and there is 4 GB available per GPU.

For each configuration, we run the relevant ray-shooting code with a fixed set of parameters (N_* , N_{pix} , N_{av}) and random number generator seed, which controls the locations of the lenses and the light rays. In order to maximise the memory available for lenses and light rays, we set all lenses to have the same mass - see section 3.2. We expect the accuracy of calculations with each code to be the same, as all use single precision floating point numbers. This was confirmed by comparing the magnification maps for each run: we choose the 1GPU map as our fiducial result, and determine the pixel-by-pixel residual for the other magnification maps. In each case, when the lens distributions are the same and the light ray positions are the same, the residual is zero for every pixel for each of the processing configurations. This demonstrates that our implementation of the algorithm across the GPU and Tesla hardware is identical to the 1CPU version. An example map is shown in Figure 1 for $N_* = 100$, $N_{\text{pix}} = 1024^2$ and $N_{\text{av}} = 1000$. To obtain timing results, we run

⁹ NVIDIA quote a peak above 500 Gflop/s on this GPU, however, this assumes that MUL and MAD instructions can be dual-issued – to our knowledge this is not possible with the 8800 GT.

¹⁰ http://www.nvidia.com/object/product_tesla_s1070_us.html

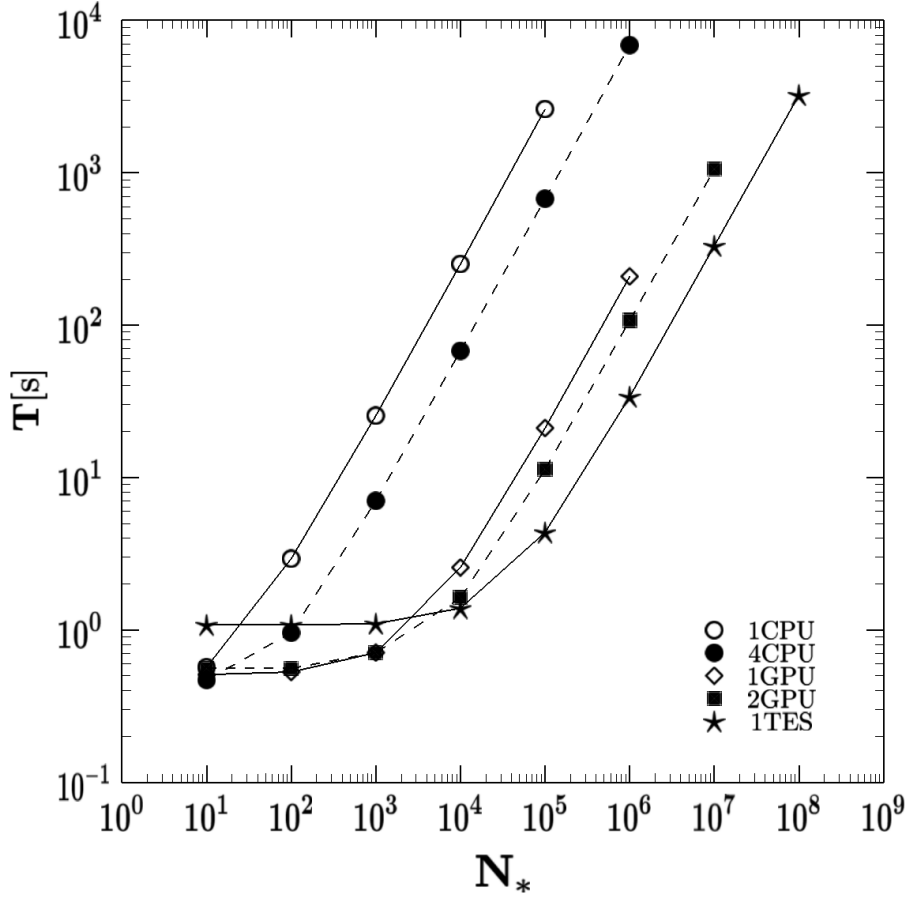


Fig. 2. Time (T [s]) taken to generate magnification maps with each of the processing configurations. The number of lenses is varied over the range $10 \leq N_* \leq 10^8$, while $N_{\text{av}} = 100$ and $N_{\text{pix}} = 192^2$ are kept fixed for each run. Each plotted value is the median of three independent runs, variation between runs was below 0.5%. Symbols are 1CPU (open circle), 4CPU (filled circle), 1GPU (open diamond), 2GPU (filled square) and 1TES (star).

each simulation three times from a different random initial configuration, and quote the median processing time, determined by generating a time stamp at the start and end of processing. We find run-time variations of between 0.1 – 0.5% across all of the simulations.

Figure 2 show results of timing tests over a range of N_* . To keep 1CPU processing times manageable, we use a small source grid with $N_{\text{pix}} = 192^2$ pixels and $N_{\text{av}} = 100$. Above $N_* = 100$, the 1CPU solution shows the expected linear scaling $\propto N_*$, as equation (2) is additive in the total number of lenses. Due to the need to move data from CPU memory to GPU memory, the GPUs and Tesla have slightly higher overheads, which mean they have reduced performance for low N_* . The linear scaling of processing time with N_* is not seen until $N_* \geq 10^4$ for 1GPU and $N_* \geq 10^5$ for 1TES.

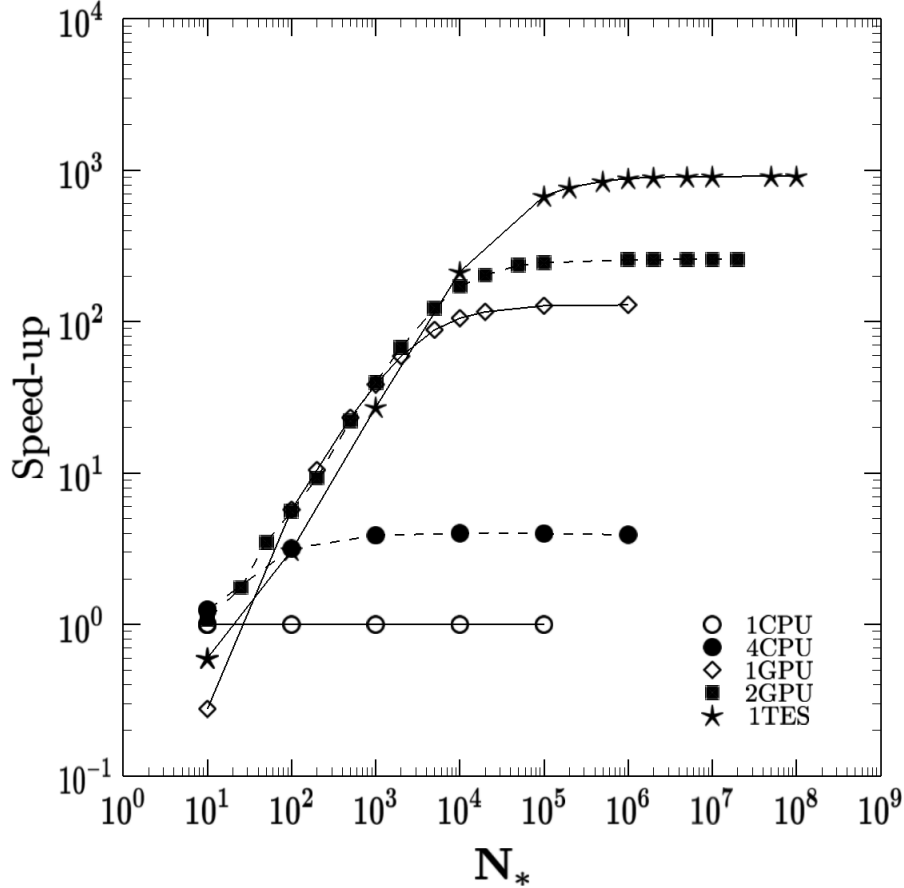


Fig. 3. Processing speed-up relative to 1CPU configuration as the number of lenses is varied over the range $10 \leq N_* \leq 10^8$, with $N_{\text{av}} = 100$ and $N_{\text{pix}} = 192^2$. Each plotted value is the median of three independent runs, variation between runs was below 0.5%. Symbols are 1CPU (open circle), 4CPU (filled circle), 1GPU (open diamond), 2GPU (filled square) and 1TES (star). Peak performances achieved were 1.4 Gflop/s (1CPU), 5.6 Gflop/s (4CPU), 182 Gflop/s (1GPU), 364 Gflop/s (2GPU) and 1287 Gflop/s (1TES). Note that the 1CPU peak is assumed to apply beyond $N_* = 10^5$, and the maximum performance improvement for the GPU configurations occurs when $N_* \geq 10^5$.

Figure 3 shows the relative speed-up in processing time compared to the 1CPU configuration as the number of lenses is varied in the range $10 \leq N_* \leq 10^8$, with $N_{\text{pix}} = 192^2$ and $N_{\text{av}} = 100$. For each processing configuration, there is a problem-size where the performance reaches a plateau level. In calculating speed-ups for the GPU systems, we assume that the 1CPU peak applies beyond $N_* = 10^5$. At $N_* = 10^4$, 1CPU and 4CPU plateau at 1.4 Gflop/s and 5.6 Gflop/s respectively; while 1GPU, 2GPU and 1TES reach their peak performance of 182 Gflop/s, 364 Gflop/s and 1287 Gflop/s respectively for $N_* \geq 10^5$. For low N_* , the extra overheads in transferring data to and from the GPU memory impacts on the total processing time. In order to achieve the greatest

Table 2

Time taken to generate magnification maps for each of the hardware configurations for varying N_{pix} , with $N_{\text{av}} = 100$, $N_* = 10^6$ fixed. Numbers in [] brackets are estimated times for large maps which would be impractical to calculate. Times are in hours.

N_{pix}	1CPU	4CPU	1GPU	2GPU	1TES
192^2	7.5	1.91	0.06	0.03	0.01
512^2	[55]	[14]	0.40	0.20	0.06
1024^2	[200]	[55]	1.59	0.80	0.23
2048^2	[850]	[200]	6.35	3.20	0.93
4096^2	[3400]	[850]	25.4	12.8	3.74
8192^2	[13700]	[3400]	[100]	50.4	14.75

performance gains compared to the CPU implementation, GPUs need large problems to solve.

Table 2 and Figure 4 show the processing times for calculating magnification maps over a range of grid sizes with $N_* = 10^6$. Numbers in [] brackets are estimated times for large maps which would be impractical to calculate with the 1CPU or 4CPU codes. The 2GPU code can calculate a $N_{\text{pix}} = 4096^2$ pixel grid in 13 hours, while 1TES can calculate a four-times larger grid in about the same time. While 1TES contains 4 GPUs, it can calculate more than 2x faster than 2GPU as each Tesla GPU gives approximately the same performance as 2GPU. As with processing times for varying N_* , we find that processing also scales linearly with N_{pix} as expected.

3.2 Other lens models

A slight modification to the lens equation, which considers the effects of the macro-model shear, γ , and surface mass density, σ , is

$$\mathbf{y} = \begin{pmatrix} 1 - \gamma & 0 \\ 0 & 1 + \gamma \end{pmatrix} \mathbf{x} - \sigma_c \mathbf{x} - \sum_{i=1}^{N_*} m_i \frac{(\mathbf{x} - \mathbf{x}_i)}{|\mathbf{x} - \mathbf{x}_i|^2} \quad (6)$$

where $\sigma = \sigma_c + \sigma_*$ combines contributions from continuously distributed matter, σ_c , and compact objects, σ_* . Since shear and convergence effectively apply a scaling factor to the ray, which can be performed as part of the accumulation stage, it neither significantly affects computation time nor requires increased memory usage. Ten years ago, Wambsganss (1999) stated that a direct inverse ray-shooting calculation for $N_{\text{pix}} = 2500^2$, $N_{\text{av}} = 500$ and $N_* = 10^6$, relevant for the astrophysically-motivated case of $\sigma_* \sim 1$ in equation (6), was impracti-

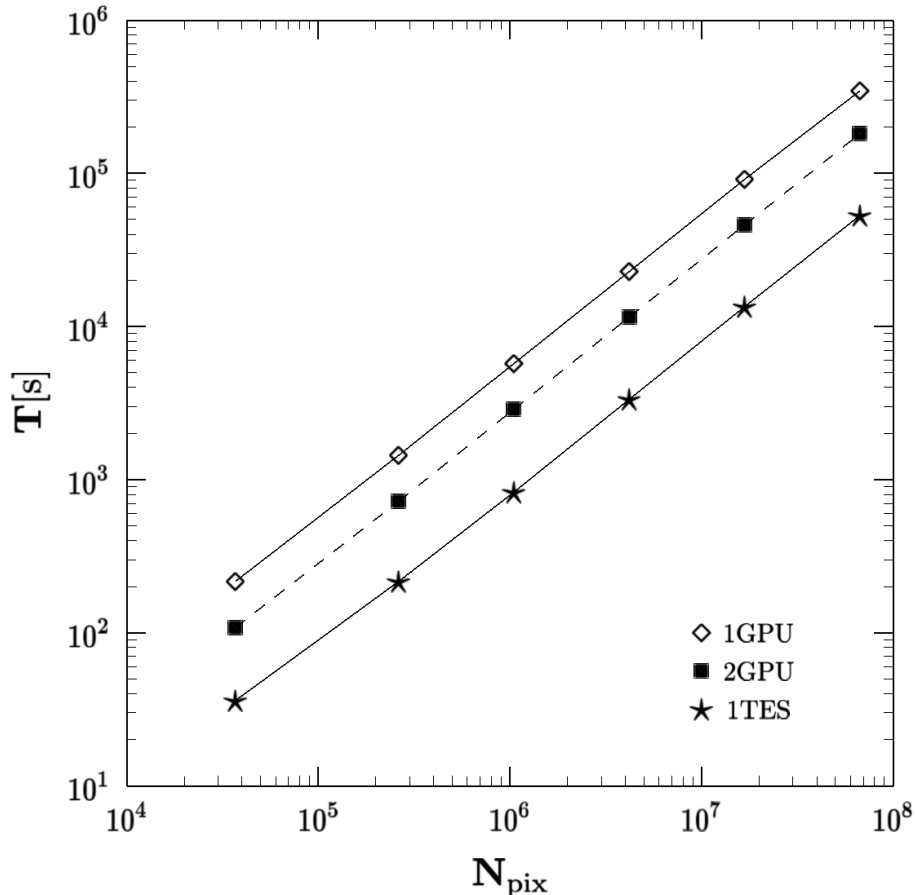


Fig. 4. Time (T [s]) taken to generate magnification maps as the number of pixels in the source grid is varied over the range $192^2 \leq N_{\text{pix}} \leq 8192^2$. The other lens parameters are kept fixed at $N_{\text{av}} = 100$ and $N_* = 10^6$. Each plotted value is the median of three independent runs, variation between runs was below 0.5%. Symbols are 1GPU (open diamond), 2GPU (filled square) and 1TES (star).

cal as “[e]ven with the fastest computers such a brute force calculation would take months or years!” With an NVIDIA S1070 Tesla unit, this brute force calculation can be achieved in ~ 7 hours.

Of more importance is the impact of allowing a variable lens mass, which does require more memory usage: a third floating point number must be stored for the mass of each lens. This means the maximum number of lenses that a single GPU can store is decreased by 33%. While computation of variable lens mass does not take any additional floating point operations, it does require an additional memory look up per lens, increasing the total number of array look ups from two to three. Tests completed over a range of N_* found a runtime increase of approximately 17% and 7% for 1GPU and 1TES respectively. The fact that a 50% increase in memory did not lead to a 33% drop in speed suggests that this computational problem is not memory bound.

3.3 Billion-lens ray-shooting

To compute N_* greater than the available memory, it is necessary to partially calculate each light ray of a subset of lenses and sum the result after computation is complete across all lenses. This can be approached in two ways, by loading and unloading lenses from GPU device memory, or by computing rays across multiple GPUs and transferring ray coordinates between GPUs. Use of multiple GPUs is limited by the number of GPUs available and their device memory, while loading and unloading lenses is limited by system memory, storage space and overheads in transferring lens data to and from the GPU.

We modify the algorithm of Section 2.3 to stage data and pass light rays sequentially through the series of 4 GPUs (numbered 1–4) in the Tesla unit. Lens coordinates are pre-loaded onto each GPU, and the first batch of light rays is loaded from system memory to GPU-1. Once deflection calculations are completed on GPU-1, the partially-deflected light rays are transferred to GPU-2, and computation is resumed. Meanwhile, the next batch of light rays is loaded onto GPU-1. This staging process continues until all light ray deflections have been calculated, allowing the final accumulation process, and magnification map generation, to be completed on the CPU. Staging ensures that there is always data ready to be processed and that the GPUs are kept utilised (except at the very start and end of the entire calculation, when light rays are first being passed to or from waiting GPUs).

With this modification to our CUDA code, we ran a ray-shooting simulation with $N_* = 10^9$, $N_{\text{pix}} = 512^2$ and $N_{\text{av}} = 42$. The calculation was completed in 23.83 hours, with a sustained rate of 1.28 Tflop/s. This indicates there is no significant overhead due to increased memory transfers and times when not all GPUs are being utilised. An additional test with $N_* = 2 \times 10^9$ was completed in 47.72 hours, also at 1.28 Tflop/s, showing that processing time is still scaling linearly with N_* .

4 Discussion

We have achieved 1.28 Tflop/s computation of gravitational lensing magnification maps by using a Tesla unit attached to a single desktop workstation. For a single GPU we are reaching 54% of the processing peak, and 52% for the Tesla. Other work, such as N -body simulations and graphic-card clusters for astrophysical simulations have achieved peak sustained performance of 223 Gflop/s (Levit & Gazis 2006), 236 Gflop/s (Belleman, Bédorf & Portegies Zwart 2008) and 256 Gflop/s (Hamada & Iitaka 2007) with an NVIDIA GeForce 8800 GTX card. The 8800 GTX has a peak of 346 Gflop/s, so these

algorithms are using up to 74% of available processing power.

It is desirable to quote the processing improvements that GPUs can provide over CPU implementations of astronomy algorithms, but care must be taken that the comparison is a fair and relevant one. In this work, we have not considered the relative performance of GPU versus hierarchical tree-codes (Wambsganss 1990, 1999) or polygon mapping methods (Mediavilla 2006). In order to isolate the performance enhancements of the GPU over a single CPU, we have deliberately used a simple “brute force” ray-shooting code, with no additional optimisation. In future work, we will address comparisons between a cluster-based hierarchical code (Garsden & Lewis 2009) and the GPU approach for billion-lens configurations.

As with previous GPU-astronomy, the difference between the actual Gflop/s obtained and the quoted peak occurs due to the nature of astronomy algorithms: in general they make use of more than just MAD instructions, which would be required to obtain maximum possible performance. For the multi-Schwarzschild lens, we have $N_{\text{flop}} = 10$ in our algorithm analysis (see appendix A), with division counted as a single flop. However, the calculation of division on an ALU takes $O(10)$ cycles, compared with a single cycle for MAD. In addition to the computation, the loop counter must be incremented and lens coordinates must be retrieved from shared memory, adding a small overhead. Given these factors, it is not surprising that we cannot reach the processing peak.

We find that incremental improvements to the processing speed can be made through judicious use of the device, shared and register memory. To maximise performance, overheads from accessing device and shared memory need to be minimised. One way to achieve this for device memory is via coalesced transfers, where there is a one-to-one mapping between threads and memory - each thread accesses its own unique device memory location, up to the maximum number of threads. This is then repeated until all the required device memory content has been transferred to shared or register memory. The GPU ray-shooting algorithm uses registers to store the ray coordinates and shared memory to store the lenses. Since the ray coordinates are accessed frequently it is advantageous to store them as registers as it allows maximum throughput; lens coordinates are better stored in shared memory, so they can be shared between threads, reducing the number of requests to device memory, as they are only accessed once per thread.

Our comparison between GPU and CPU codes does not consider an obvious optimisation that is reasonably straightforward on today’s CPUs. Modern CPUs typically have word widths of order 128 or 256 bits. This allows them (for example) to pass up to four single precision (32-bit) floating point values through the processor on each clock cycle. In this example, single-instruction

multiple data (SIMD) instructions could be issued to the CPU’s arithmetic logic unit to treat the 128-bit word as four single-precision floating-point numbers. The same floating point operation would be applied to each number, taking the same number of clock cycles that an operation on just one number would consume. In the ideal case, this can quadruple the floating-point speed of a *CPU-bound* program. However, the *practical* benefit of re-writing CPU code using SIMD extensions is often less than a factor of four: simple mathematical operations such as addition and multiplication are actually *memory bandwidth-bound* on contemporary architectures such as the Intel Xeon E5345, so unless longer-cycle operations such as reciprocal and reciprocal-square-root are in frequent use, the benefit of SIMD operations is limited.

Most currently available GPUs have extremely limited ability to perform computation with double precision (64-bit) floating point numbers: the NVIDIA G200 series and Tesla S1070 can typically only run double precision calculations at a fraction of the single precision rate (e.g. double precision processing occurs at ~ 300 Gflop/s on the Tesla, compared to 2.488 Tflop/s for single precision). Typical three-dimensional graphics processing does not require double precision, and as a result, this has not been a priority for hardware development. Due to the stochastic nature of the inverse ray-shooting method (random lens positions and random ray positions), the additional accuracy introduced by a move to double precision is not critical (however, this may become more of an issue when comparing with a hierarchical tree-code). As the market for GPGPU work grows, it is probable that (faster) double precision will become a standard feature. In the meantime, careful scheduling of calculation can be used so that double precision is only used for those parts of the calculation that require it.

These discussions of algorithm comparisons notwithstanding, the processing speed-ups enabled with GPUs provides scope to consider improvements to the way microlensing problem-space is addressed, and opportunities for real-time computation. In section 1, we introduced Φ as a count of the number of calculations required for direct ray shooting. Φ is often kept manageable by foregoing any repeat map generations (i.e. $n = 1$), but this neglects the role of dynamic effects: static magnification maps do not account for the motion of individual stars, which can have a dramatic impact on the configuration of the caustic network over short timescales (Schramm et al. 1993), and may be a cause of rapid microlensing variability (Schechter et al. 2003; Kochanek et al. 2007). An additional limitation of using a single magnification map is that all light curves are not statistically independent as source trajectories keep crossing the same set of caustics, however, it has not been feasible to produce a different magnification map for each sample light curve. The order of magnitude improved performance of GPU-based systems over the CPU-only case makes multiple-map generation (with direct calculations) a practical option – even for very large N_* scenarios.

Over a useful range of N_* and N_{pix} values, we have demonstrated that the processing times for the 1GPU, 2GPU and 1TES solutions scale linearly with these quantities. Although we do not explicitly present results, we also find linear scaling in processing time for varying N_{av} , in the regime where processors are fully utilised. In order to examine the regions of cosmological microlensing parameter space that can be accessed with a GPU implementation of ray-shooting, we rewrite results from Table 2 as scaling relations:

$$T_{1\text{GPU}} = 9.2 \times 10^4 \left(\frac{N_{\text{pix}}}{4096^2} \right) \left(\frac{N_*}{10^6} \right) \left(\frac{N_{\text{av}}}{100} \right) \text{ s} \quad (7)$$

$$T_{1\text{TES}} = 1.4 \times 10^4 \left(\frac{N_{\text{pix}}}{4096^2} \right) \left(\frac{N_*}{10^6} \right) \left(\frac{N_{\text{av}}}{100} \right) \text{ s} \quad (8)$$

If we consider a “real-time” calculation to be achievable in 60 seconds, then the 1TES solution allows us to consider problems such as $N_{\text{pix}} = 1024^2$, $N_* = 10^5$ and $N_{\text{av}} = 50$. For an interactive, quick-look at the effects of changing the lens mass distribution, or allowing time-evolving motion of lenses, computational steering with a direct ray-shooting calculation is feasible. An alternative application is the ability to interactively zoom into a magnification map: by initially starting with a low detail map, an area of interest can be selected and higher detail computed rapidly.

Finally, it is worth considering the financial cost of GPU-based ray-shooting - although these figures are somewhat rubbery. To achieve 1.2 Tflop/s with a cluster of 4CPU machines, with a peak of 5.6 Gflop/s, we would require ~ 200 four-core compute nodes. Assuming perfect networking (at zero cost!), such a facility would cost $O(\sim 300\,000)$ USD, or around 250 000 USD per Tflop/s. The 2GPU solution costs ~ 2000 USD, with a peak of 364 Gflop/s. Again, with the assumption of perfect networking, we would need four machines, at a cost of ~ 7000 USD per Tflop/s. This is comparable with the 8000 USD per Tflop/s for 1TES (based on system price of 10 000 USD), with no networking required. It is obvious that on a financial basis alone, the GPU-based solutions offer several orders of magnitude savings compared to CPU-clusters to achieve a particular processing goal. What is not yet known is how many other astronomy algorithms can benefit as significantly from a GPU-implementation as the ray-shooting case – this will be the subject of future work.

5 Conclusions

We have demonstrated the benefits of applying programmable graphics hardware to a common problem in gravitational lensing: the creation of microlensing magnification maps. Multi-GPU ray-shooting can provide low-cost, Tflop/s

performance without the programming complexities of implementing a hierarchical tree code, or the financial costs associated with using a distributed computing cluster. Significantly faster compute times expand the parameter space that can be explored in cosmological microlensing experiments, and open up new opportunities for “real-time” computational steering or interaction with a microlensing simulation.

Acknowledgements

This research was supported under Australian Research Council’s Discovery Projects funding scheme (project number DP0665574). We thank the anonymous referee for suggestions that improved the presentation of results.

References

- Alcock, C., Akerlof, C.W., Allsman, R.A., Axelrod, T.S., Bennett, D.P., Chan, S., Cook, K.H., Freeman, K.C., Griest, K., Marshall, S.L., Park, H.S., Perlmutter, S., Peterson, B.A., Pratt, M.R., Quinn, P.J., Rodgers, A.W., Stubbs, C.W., Sutherland, W., 1993, *Nature*, 365, 621
- Aubourg, E., et al., 1993, *Nature*, 365, 623
- Barnes, J., Hut, P. 1986, *Nature*, 324, 446
- Belleman, R.G., Bédorf, J., Portegies Zwart, S.F. 2008, *NewA*, 13, 103
- Elsen, E., Vishal, V., Houston, M., Pande, V., Hanrahan, P., Darve, E. 2007, arXiv:0706.3060v1 [cs.CE]
- Ford, E.B. 2008, *NewA*, 14, 406
- Fournier, A., Fussell, D. 1988, *ACM Transactions on Graphics*, 103.
- Garsden, H., Lewis, G.F., 2009, *NewA*, submitted
- Gould, A. 2008, eprint arXiv:0803.4324
- Hamada, T., Iitaka, T. 2007, arXiv:astro-ph/0703100v1
- Harris, C., Haines, K., Staveley-Smith, L. 2008, *ExA*, 22, 129
- Hjorth, J., et al. 2002, *ApJ*, 572, L11
- Irwin, M.J., Webster, R.L., Hewett, P.C., Corrigan, R.T., Jędrzejewski, R.I., 1989, *AJ*, 98, 1989
- Kayser, R., Refsdal, S., Stabell, R. 1986, *A&A*, 166, 36
- Kochanek, C.S., Dai, X., Morgan, C., Morgan, N., Poindexter, S., Chartas, G. 2007, in *Satistical Challenges in Modern Astronomy IV*, ed. G.J.Babu & E.D.Feigelson (San Francisco:ASP), 43
- Levit, C., Gazis, P. 2006, *AAS*, 208, 1904
- Lewis, G.F., Miralda-Escude, J., Richardson, D.C., Wambsganss, J., 1993, *MNRAS*, 261, 647
- Mao, S. 2008, arXiv:0811.0441v1 [astro-ph]

- Mediavilla, E., Muñoz, J.A., Lopez, P., Mediavilla, T., Abajas, C., Gonzalez-Morcillo, C., Gil-Merino, R., 2006, *ApJ*, 653, 942
- Merz, H., Pen, U.-L., Trac, H., 2005, *NewA*, 10, 393
- Moore, A.J., Quillen, A.C., Edgar, R.G., 2008, arXiv:0809.2855v1 [astro-ph]
- Mudryk, L.R., Murray, N.W., 2009, *NewA*, 14, 71
- Nyland, L., Harris, M., Prins, J.F., 2004, in *ACM Workshop on General-Purpose Computing on Graphics Processors (Poster)*, C-37
- Nyland, L., Harris, M., Prins, J.F., 2008, *GPU Gems 3*, Addison-Wesley, ch. 31, 677
- Oguri, M. 2007, *ApJ*, 660, 1
- Ord, S., Greenhil, L., Wayth, R., Mitchell, D., Dale, K., Pfister, H., Edgar, R.G. 2009, arXiv:0902.0915 [astro-ph.IM]
- Owens, J.D., Luebke, D., Govindaraju, N., Harris, M. Krüger, J., Lefohn, A.E., Purcell, T.J. 2005, *Computer Graphics Forum*, 26(1), 80
- Paczyński, B. 1986, *ApJ*, 301, 503
- Portegies Zwart, S.F., Belleman, R.G., Geldof, P.M. 2007, *NewA*, 12, 641
- Saha, P., Coles, J., Macciò, A.V., Williams, L.L.R. 2006, *ApJ*, 650, L17
- Schaaf, K.V.D., Overeem, R., 2004, *Experimental Astronomy*, 17, 287–297
- Schechter, P.L. et al. 2003, *ApJ*, 584, 657
- Schive, H.-Y., Chien, C.-H., Wong, S.-K., Tsai, Y.-C., Chiueh, T. 2007, *NewA*, 13, 418
- Schneider, P., Ehlers, J., Falco, E.E. 1992, *Gravitational Lenses* (Berlin: Springer)
- Schneider, P., Weiss, A. 1986, *A&A*, 164, 237
- Schneider, P., Weiss, A. 1987, *A&A*, 171, 49
- Schramm, T., Kayser, R., Chang, K., Nieser, L., Refsdal, S., 1993, *A&A*, 268, 350
- Semelin, B., Combes, F., 2005, *A&A*, 441, 55
- Szalay, T., Springel, V., Lemson, G., 2008, arXiv:0811.2055v2 [cs.GR]
- Thacker, R.J., 1999, PhD Thesis (University of Alberta, Canada)
- Thacker, R.J., Couchman, H.M.P., 2006, *CoPhC*, 174, 540
- Tomov, S., McGuigan, M., Bennett, R., Smith, G., Spiletic, J. 2003, arXiv:cs/0312006
- Udalski, A., Szymanski, M., Kuzlunzy, J., Kubiak, M., Krzeminski, W., Mateo, M., Preston, G.W., Paczynski, B., *Acta Astronomica*, 43, 289
- Vakulik, V., Schild, R., Dudinov, V., Nuritdinov, S., Tsvetkova, V., Burkhonov, O., Akhunov, T. 2006, *A&A*, 447, 905
- Vanderriest, C., Schneider, J., Herpe, G., Chevreton, M., Moles, M., Wlerick, G., 1989, *A&A*, 215, 1
- Venkatasubramanian, S. 2003, In *SIGMOD Workshop on Management and Processing of Massive Data*, arXiv:cs/0310002
- Wambsganss, J. 1990, PhD Thesis, MPA Report 550
- Wambsganss, J. 1999, *JCAM*, 109, 353
- Wambsganss, J. 2006, in *Gravitational Lensing: strong, weak and micro*. Saas-Fee Advanced Course 33, ed. G.Meylan, P.Jetzer, & P. North (Berlin:

Springer), 453
 Wayth, R., Dale, K., Greenhill, L.J., Mitchell, D.A., Ord, S., Pfister, H. 2007, AAS, 211, 1104
 Witt, H.J., 1993, ApJ, 403, 530
 Wyithe, J.S.B., Webster, R.L., 1999, MNRAS, 306, 223

A Counting flops

The many-Schwarzschild lens model, equation (2), requires $N_{\text{flop}} = 10$ floating point operations per calculated deflection, counted as follows:

$$\begin{aligned}
 f_1 &= x_1 - x_{i,1} && 1 \text{ flop} \\
 f_2 &= x_2 - x_{i,2} && 1 \text{ flop} \\
 d &= m_i / (f_1 \times f_1 + f_2 \times f_2) && 4 \text{ flops} \\
 \alpha_1 &= \alpha_1 + (d \times f_1) && 2 \text{ flops} \\
 \alpha_2 &= \alpha_2 + (d \times f_2) && 2 \text{ flops}
 \end{aligned}$$